Геология и геофизика, 2017, т. 58, № 11, с. 1703—1720
УДК 550.42(560/566)

ГЕОХИМИЯ МЕСТОРОЖДЕНИЙ БАРИТА ВБЛИЗИ РАЙОНА АДАНА-ФЕКЕ (*Восточная Таврида*)

А. Тас Оздоган[a], Й. Урас[b], Ф. Онер[c]

[a]*MTA Dogu Akdeniz Bolge Mudurlugu*
[b]*Kahramanmaras Sutcu Imam University, Faculty of Engineering and Architecture, Department of Geological Engineering, 46040, Kahramanmaras, Turkey*
[c]*Mersin University, Faculty of Engineering and Architecture, Department of Geological Engineering, Mersin Turkey*

Месторождения барита, проявленные в виде вен и жил внутри или вдоль контактных зон перекристаллизованных известняковых и доломитовых толщ кембрийской свиты Деджирментас, имеют эпигенетическую природу. Тип отложения баритов, их минеральные ассоциации, высокое содержание SrO и вид изменения вмещающей породы свидетельствуют об их гидротермальном происхождении. Однако на диаграммах Ce_N/Yb_N–Yb_N и Ce_N/Sm_N–Ce_N/Yb_N образцы барита располагаются вокруг поля морской воды. Данные о флюидных включениях в баритах свидетельствуют об их образовании из раствора с низкой солёностью (0.9—1.6 мас. % NaCl-экв.) при температурах гомогенизации от 78 до 190 ºС. Изотопные составы серы баритов изменяются от 32.2 до 36.3‰, а значения $^{87}Sr/^{86}Sr$ варьируют от 0.709885 до 0.749652. Тип осаждения баритов, их минеральные ассоциации, составы микроэлементов, данные о флюидных включениях и изотопные параметры $\delta^{34}S$ и $^{87}Sr/^{86}Sr$ указывают на возможное образование гидротермальных растворов из погребённой интрузии, смешении их с метеорными и морскими водами и взаимодействии с докембрийско-фанерозойскими метакластическими и кембрийскими карбонатными породами с образованием отложений барита.

Барит, редкоземельные элементы, флюидные включения, изотоп, Феке (*Адана*)

GEOCHEMISTRY OF THE BARITE DEPOSITS NEAR ADANA-FEKE AREA (*Eastern Taurides*)

Afitap Tas Ozdogan, Yusuf Uras, and Fevzi Oner

The barite deposits that emerge as veins and lodes within or along the contact zones of recrystallized limestone and dolomite units of Cambrian Degirmentas Formation are of epigenetic character. Depositional styles, paragenesis, host rock alteration styles, and high SrO contents of the barites suggest a hydrothermal origin for their formation. However, considering their rare earth element compositions, barite samples surround the field for seawaters when plotted on Ce_N/Yb_N–Yb_N and Ce_N/Sm_N–Ce_N/Yb_N diagrams. Fluid inclusion data obtained from the barites indicated a formation from a fluid with low salinity (0.9–1.6 wt.% NaCl eq.) at homogenization temperatures between 78 and 190°C. Sulfur isotopic compositions of barites vary between +32.2 and +36.3‰, and their $^{87}Sr/^{86}Sr$ values range between 0.709885 and 0.749652. Depositional styles, parageneses, trace element compositions, fluid inclusion data as well as $\delta^{34}S$ and $^{87}Sr/^{86}Sr$ isotopic data indicate a model in which hydrothermal fluids were possibly derived from a buried intrusion mixed with meteoric and marine waters, further interacting with the Precambrian – Phanerozoic metaclastic and Cambrian carbonate rocks to form barite deposits.

Feke (Adana), barite, rare earth elements, fluid inclusions, isotope

1. INTRODUCTION

Barite deposits that have been observed near Feke in the eastern Taurides emerge as economical vein- and lode-type deposits within the rocks of the Middle Cambrian Degirmentas Formation. Barite deposits are regionally aligned along NE–SW direction with dips towards SW and NE, and they vary in thickness between 4 and 6 m and in lengths between 50 and 100 m. Ozus and Yaman (1986) studied the depositional processes and sources of the barite deposits that are found in the regions including those which are located in the current study area, and indicated that these vein-type barite deposits were formed from a combination of sedimentary, diagenetic, remobilization, and tectonic processes. According to their findings, elements contained in these deposits were remobilized from either the sedimentary rocks or formation water by groundwater, and they were epigenetically deposited along the fracture systems later. According to a second study, the regional fluorite deposits associated with these barite mineralizations were formed with hydrothermal processes (Uras et al., 2003).

2. GEOLOGICAL SETTING

The study area covers the plateau that lies between Kozan, Feke and Mansurlu regions of Adana Province (Figure 1). Emirgazi group in the study area consists of two formations, Kozan Formation and the overlying

© **А. Тас Оздоган✉, Й. Урас, Ф. Онер, 2017**
✉e-mail: afitapt@hotmail.com
DOI: 10.15372/GiG20171106

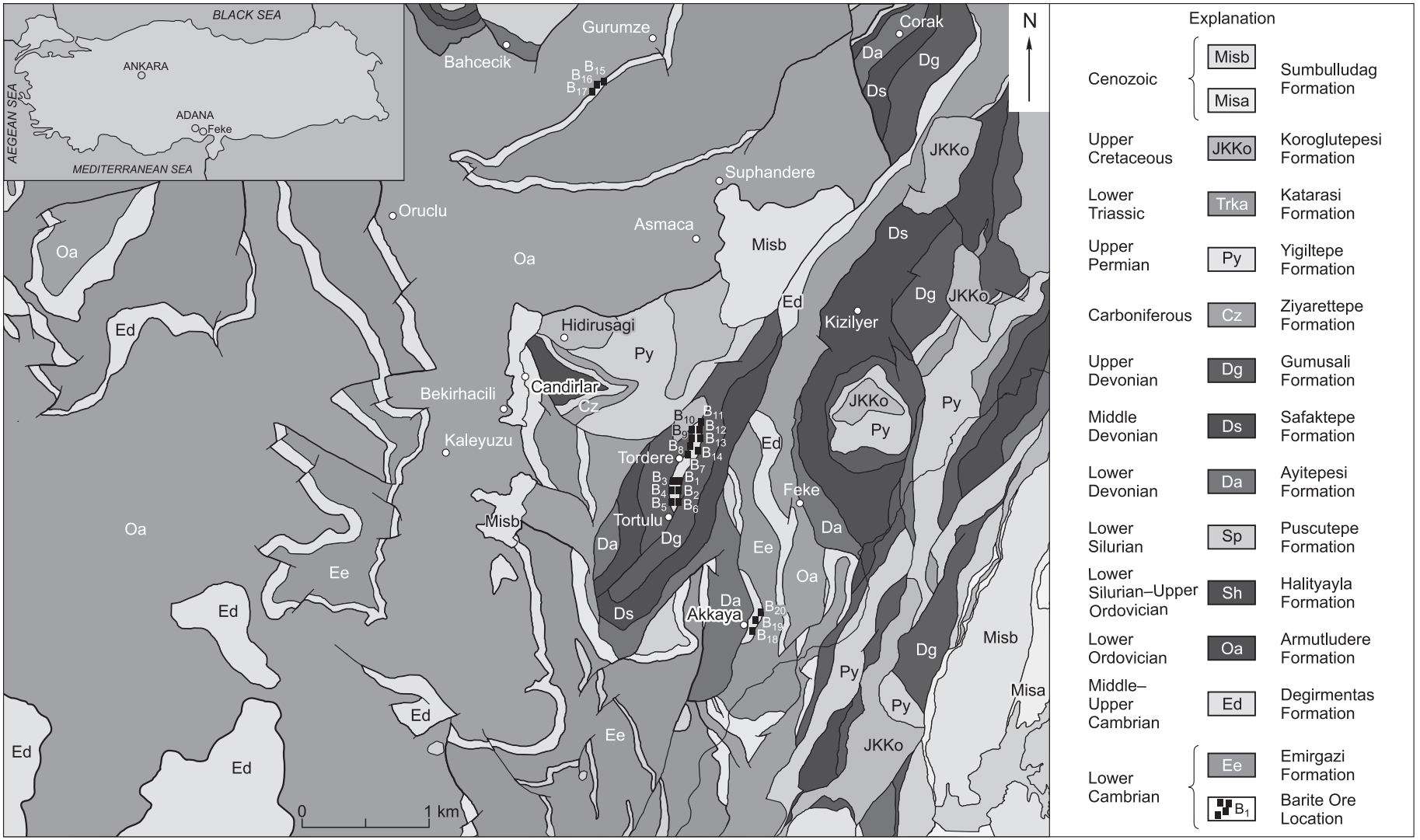

Fig. 1. Geological location map of Feke (Adana) - the surrounding area (Ayhan, 1988).

Kocyazi Quartzite (Ozgul and Kozlu, 2002). The latter is conformably overlaid by the Degirmentas Formation. This unit consists of a thick carbonate sequence of laterally transitional (and locally alternating) dolomite, dolomitic limestone, neritic limestone and thinly-intercalated shale, and nodular limestone from bottom to top. The dolomite is gray, coarsely crystalline, medium-bedded and often fractured with calcite infillings, and the limestone is light to dark gray and locally white, medium-bedded and displays recrystallization textures. The latter unit hosts the barites. The Ordovician Armutlu Formation overlies the Degirmentas Formation. On a geological map, the Degirmentas Formation is bound by a series of dip slip faults representing the tectonic contacts with the Yigilitepe and Safaktepe Limestone Formations. Halityaylasi Formation was created in a shallow and high-energy setting. The Puscutepe Formation is represented by gray-black colored, thinly-bedded and laminated, graptolite-rich shale. It is in compliance with the underlying Halityaylasi Formation, and passes into the Yukariyayla Formation at the top. In the study area, Ayitepesi Formation, Safaktepe Formation, Gumusali Formation, Ziyarettepe Formation, Yigilitepe Formation, Katarasi Formation , Koroglu Tepesi and Sumbuldagi Formation are observed respectively. These orebodies are located within the borders of Akkaya, Tortulu, Tordere and Bahcecik villages (Figure 2). The barites occur either as veins or lodes emplaced within the fracture zones or open spaces along the fault zones cross-cutting the limestone or dolomitic limestone beds, or as NE–SW-trending discordant layers along the bedding planes of the same lithology types that belong to the Degirmentas Formation of Middle to Late Cambrian Period. Additionally, numerous uneconomic

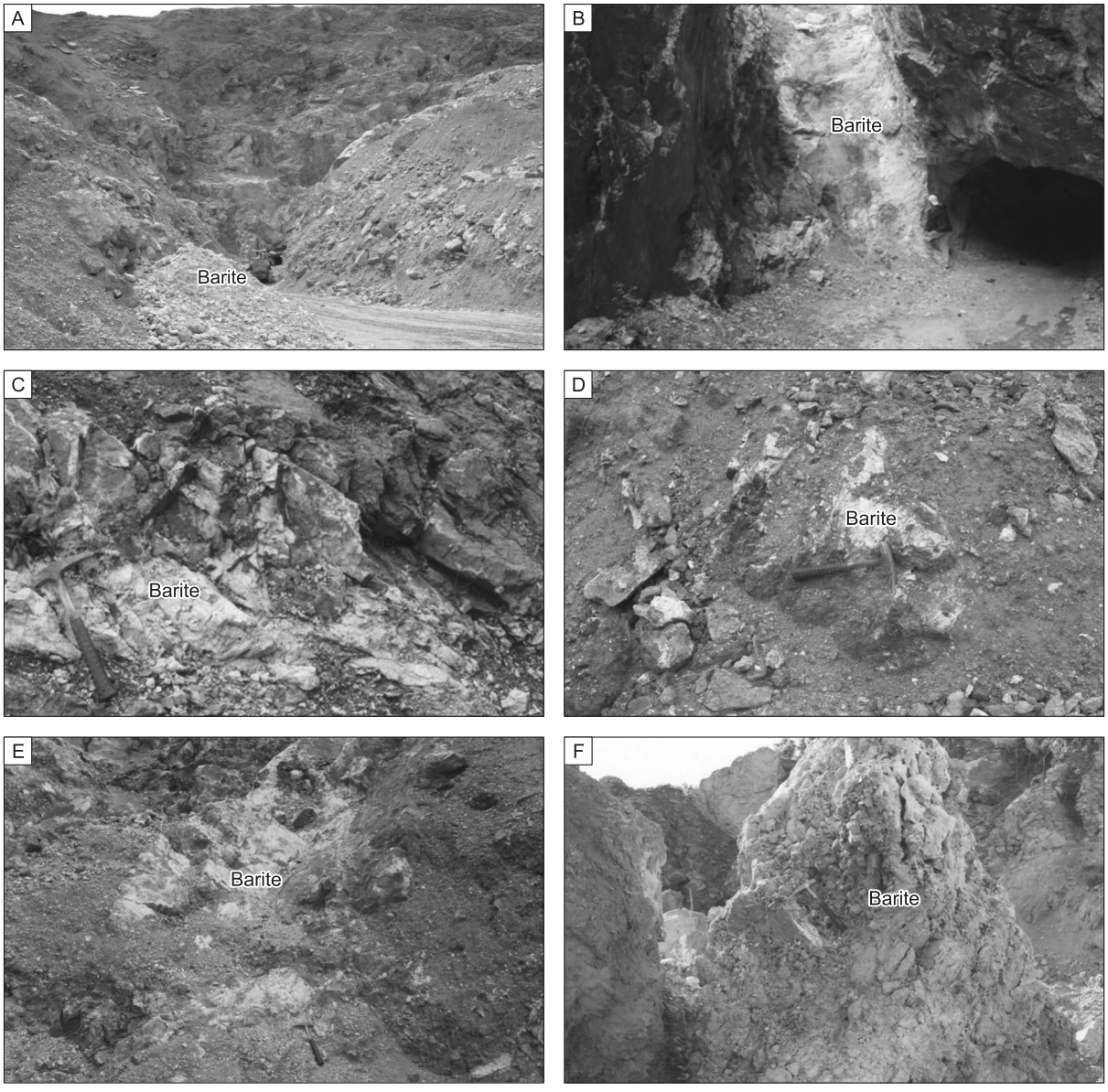

Fig. 2. General view of the barites. A. Tortulu barites, B. Tordere barites, C. Akkaya barites, D. Candırlar barites, E. Suphandere barites, F. Bahcecik barites.

vein- and lode-type mineralizations are present throughout the study area, particularly near Candirlar (Taslik Hill) and Suphandere areas (Figure 2). These barite masses were developed along irregular fractures and cracks, and have undergone tectonic deformation.

3. MINERALOGY

Petrographic investigations indicated that coarse-grained anhedral barite crystals have been broken and recrystallized along their fracture planes due to tectonism (Figure 3), forming euhedral microcrystalline barite of secondary origin. Thus, there are two different generations of barite identified in the samples. In order to determine the mineralogical compositions, a total of twenty samples collected from the study area were analyzed using the X-ray diffraction (XRD) technique. Representative XRD diagrams of some samples are provided in Figures 4.A and 4.B. XRD analysis of the barite samples indicated a predominant mineral assemblage of barite ($BaSO_4$), calcite ($CaCO_3$), and quartz (SiO_2), whereas the host rocks mainly consist of calcite, quartz, dolomite, and minor amounts of mica, fluorite, feldspar, and amphibole.

4. ANALYTICAL METHODS

Thin sections were used to determine the mineralogical and textural characteristics of the samples and to study the fluid inclusions, XRD, and some of the major and trace element analyses using XRD were carried out in the Mineralogy-Petrography Laboratory of the Mineral Research and Exploration Institute of Turkey (MTA). A total of 15 clear looking and coarsely-crystalline barite samples were collected from the barite deposits in the study area, but only 5 of these samples were deemed suitable for fluid inclusion analysis. Geochemical analyses

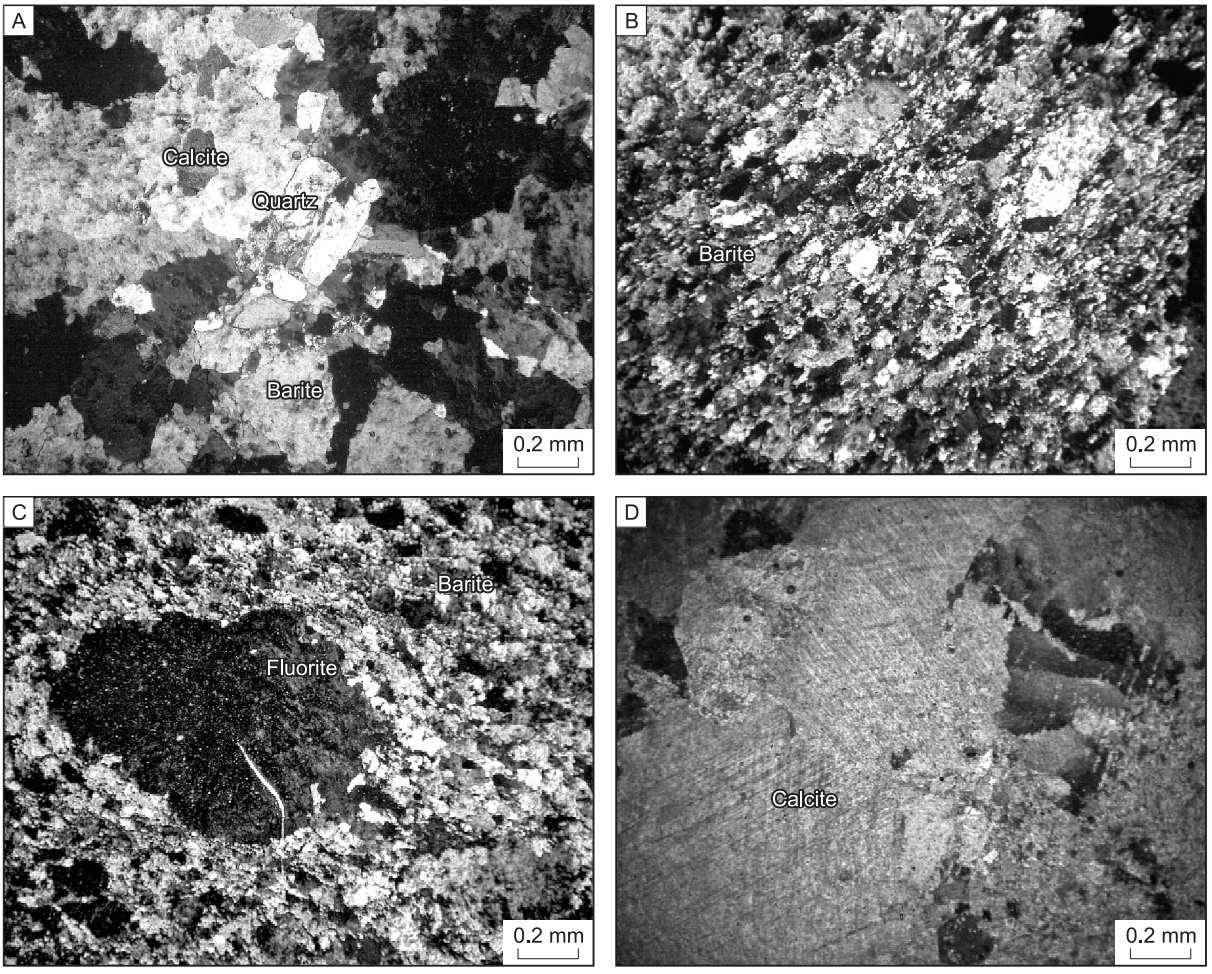

Fig. 3. A. Anhedral barite crystals have been broken and recrystallized along their fracture planes due to tectonism, B. Some of the broken barite crystals, which have been cemented by microcrystalline barites, display breccia-like textures, C. Sparse fluorite was identified as accompanying barite crystals, D. In the host rocks, calcite grains were identified as often displaying pressure twins, locally together with quartz and opaque minerals.

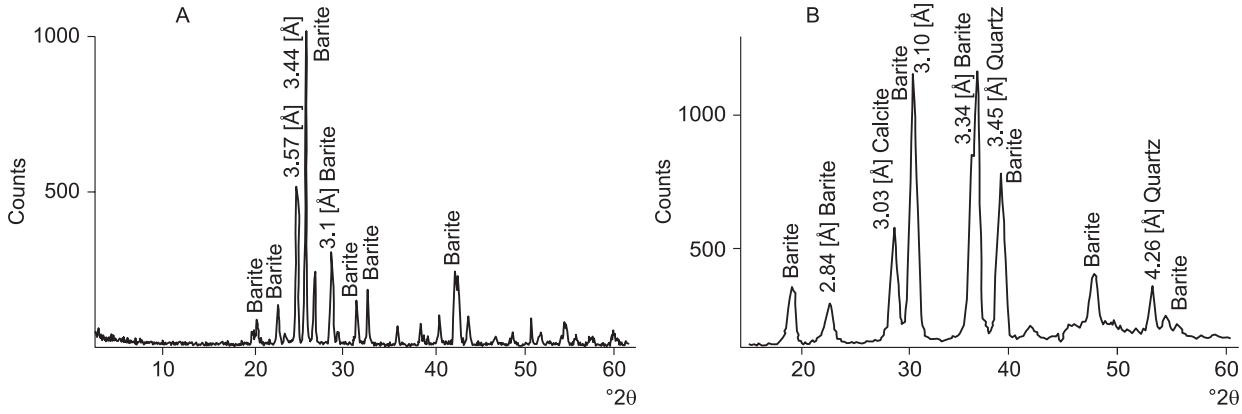

Fig. 4. A. XRD diagrams of barite sample, B. XRD analysis of the barite samples indicated a predominant mineral assemblage of barite ($BaSO_4$), calcite ($CaCO_3$), and quartz (SiO_2).

of the barite samples were performed at the ACME Analytical Laboratories (Canada), and isotopic analyses were carried out at the Geochron Laboratories Div. Krueger Enterprises Inc. (USA).

5. RESULTS

5.1. Geochemistry

A total of 38 samples that were collected from the barite deposits and orebodies seen in the study area were analyzed for their major, trace, and rare earth element compositions. In some ore samples, SiO_2 contents varied between 1 and 3 wt.%, whereas in other samples SiO_2 was scarce with similar values (Tables 1 and 2).

Samples have low Al_2O_3, Fe_2O_3, MnO, MgO, CaO, Na_2O, K_2O, TiO_2, and P_2O_5 contents, but this could not be attributed to any specific mineral phase. The BaO contents of the barite ores range between 62.99 and 59.35 wt.%, whereas their SrO levels are between 1.02 and 2.28 wt.% (Table 1). The high presence of strontium in barite deposits is related to the similarities in the atomic radii of strontium and barium, which leads to isomorphic replacement of barium found in barite crystals by strontium. The above mentioned presences of these

Table 1. **Major element contents of the studied barites (values are presented in percentage)**

Mineral Deposits	Sample	BaO	SrO	SiO_2	Al_2O_3	Fe_2O_3	MgO	CaO	Na_2O	K_2O	TiO_2	P_2O_5	MnO	SO_3	LOI
Tortulu	T-B1	62.65	1.92	<.01	0.01	0.05	<.01	0.03	<.01	<.01	<.01	<.001	<.01	35.06	0.3
	T-B2	62.49	2.28	0.04	<.01	<.04	<.01	0.77	<.01	<.01	<.01	<.001	<.01	34.43	0
	T-B3	63.13	1.51	0.06	0.02	0.09	<.01	0.41	<.01	<.01	<.01	<.001	<.01	34.41	0.3
	T-B4	62.37	1.02	0.12	<.01	0.05	<.01	0.9	<.01	<.01	<.01	<.001	<.01	34.66	0.7
	T-B5	62.58	1.17	0.27	0.11	0.85	0.01	0.32	<.01	0.03	<.01	0.01	<.01	34.11	0.4
	T-B6	60.22	1.55	2.12	0.03	0.62	0.01	1.87	<.01	<.01	<.01	<.001	<.01	32.89	0.6
Tordere	TD-B7	61.51	1.21	3.28	0.09	0.24	0.02	0.35	<.01	0.02	<.01	<.001	<.01	33.04	0.1
	TD-B8	62.92	1.83	0.02	<.01	0.07	0.01	0.03	<.01	<.01	<.01	<.001	<.01	35.01	0.1
	TD-B9	62.74	1.87	0.03	0.1	0.08	0.01	0.03	<.01	<.01	<.01	<.001	<.01	35.03	0.1
	TD-B10	62.86	1.93	0.17	0.01	0.48	<.01	0.26	<.01	<.01	<.01	<.001	<.01	34.18	0.1
	TD-B11	62.65	1.78	0.15	<.01	0.05	0.01	0.34	<.01	<.01	<.01	<.001	0.01	34.88	0.1
	TD-B12	62.62	1.77	0.25	0.09	0.23	0.02	0.36	<.01	0.02	<.01	<.001	<.01	34.21	0.4
	TD-B13	59.35	1.02	0.12	0.05	0.31	0.39	3.37	<.01	<.01	<.01	<.001	0.02	31.99	3.2
	TD-B14	62.57	1.89	0.31	0.12	0.8	<.01	0.03	<.01	0.03	<.01	<.001	<.01	34.13	0.1
Bahcecik	B-B15	62.68	1.91	0.16	0.01	0.05	<.01	0.8	<.01	<.01	<.01	<.001	0.02	34.26	0.1
	B-B16	62.66	1.91	0.04	0.01	0.04	<.01	0.2	<.01	<.01	<.01	<.01	<.01	35.03	0.1
	B-B17	62.99	2.21	0.03	0.02	0.05	<.01	0.4	<.01	<.01	<.01	<.01	<.01	34.23	0.1
Akkaya	A-B18	61.99	2.03	2.2	0.01	0.02	<.01	0.2	<.01	<.01	<.01	<.01	<.01	33.46	0.1
	A-B19	62.64	1.93	<.01	0.01	0.05	<.01	0.03	<.01	<.01	<.01	<.001	<.01	35.03	0.3
	A-B20	62.89	1.94	0.17	0.01	0.48	<.01	0.26	<.01	<.01	<.01	<.001	<.01	34.76	0.1

Table 2. **Trace element contents of the studied barites (Barite values are presented in percentage. Amount of other elements are presented in ppm)**

Mineral Deposits	Sample	Ba %	Sr	Ni	Co	Hf	Nb	Rb	Ta	Zr	Y	Cu	Pb	Zn	As	Cd	Ag
Tortulu	T-B1	56.14	16238	26	0.3	0.7	0.1	<.1	1.6	0.8	1.2	0.4	0.3	1	<.5	<0.1	<0.1
	T-B2	55.99	19270	22	0.2	0.6	<.1	<.1	2.2	0.2	1.4	1	0.3	1	1.1	<0.1	<0.1
	T-B3	56.57	12801	<20	<.2	0.9	<.1	0.1	2.8	0.2	1.5	0.6	0.3	2	<.5	<0.1	<0.1
	T-B4	55.89	8675	25	0.2	0.7	0.1	<.1	2	0.1	1.5	0.3	0.8	3	<.5	<0.1	<0.1
	T-B5	56.07	9899	21	0.5	1.2	0.2	1.1	2.7	1.3	1.6	0.3	1	1	<.5	<0.1	<0.1
	T-B6	53.96	13126	21	1.2	1	0.1	0.2	2.4	0.4	2.3	6.7	7.7	1	15.4	<0.1	<0.1
Tordere	TD-B7	55.11	10219	25	2.8	0.9	0.2	1.1	2.4	1.5	1.3	5.9	1.5	1	2	<0.1	<0.1
	TD-B8	56.38	15456	20	0.2	0.6	0.1	0.1	1.5	0.2	1.2	0.4	0.3	1	1.1	<0.1	<0.1
	TD-B9	56.22	15789	22	1.1	0.8	0.2	1	2.3	0.3	1.3	0.5	0.5	1	1.2	<0.1	<0.1
	TD-B10	56.32	16345	<20	1.2	1	0.1	0.1	3	0.2	1.7	0.7	2.2	2	<.5	<0.1	<0.1
	TD-B11	56.14	15034	21	0.5	0.9	<.1	<.1	2.6	0.4	1.3	0.3	2.1	3	<.5	<0.1	<0.1
	TD-B12	56.11	14987	24	0.3	1	<.1	<.1	2.9	0.6	1.7	0.4	0.6	2	<.5	<0.1	<0.1
	TD-B13	53.18	8690	21	0.7	1	0.1	0.5	2.2	0.5	1.9	1	13.5	2	2.4	<0.1	<0.1
	TD-B14	56.07	15981	25	0.4	1.1	0.1	0.3	2.1	0.2	1.6	0.8	1.9	1	2.6	<0.1	<0.1
Bahcecik	B-B15	56.17	16157	20	1.3	0.7	0.1	0.2	2.5	0.4	1.2	0.5	0.7	1	<.5	<0.1	<0.1
	B-B16	56.15	16122	21	0.3	0.6	0.1	<.1	2.1	0.2	1.2	0.4	0.3	1	<.5	<0.1	<0.1
	B-B17	56.45	18680	22	0.2	0.7	0.1	<.1	2.2	0.4	1.2	0.3	0.5	1	<.5	<0.1	<0.1
Akkaya	A-B18	55.55	17123	23	0.2	0.5	0.1	<.1	2	0.3	1.2	0.4	0.3	1	<.5	<0.1	<0.1
	A-B19	56.13	16342	26	0.3	0.7	0.1	<.1	1.6	0.8	1.2	0.4	0.3	1	<.5	<0.1	<0.1
	A-B20	56.36	16445	<20	1.2	1	0.1	<.1	3	0.2	1.7	0.5	2.2	2	<.5	<0.1	<0.1

two elements imply that Sr concentrations obtained from the barite samples can be used to determine the genesis of the deposit. Barite samples from the study area have SrO contents that are similar to those of many other hydrothermal barite deposits.. Some barite deposits in Turkey and other countries are present in the % SrO values (Figure 5).

Analysis toward the trace elements of barites indicated low concentration values for elements including Y, Ni, and Co (Table 2). The Pb contents of the barites in samples B6, B13, and B21 range between 7 and 13.5 ppm, and the remaining samples have lower Pb concentrations (Table 2). Zn concentrations are between 1 and 3 ppm, whereas Cu presences average between 0.4 and 6.7 ppm. Cd and Ag contents, on the other hand, are below detection limits. The host limestones from the study area have Pb and Zn concentrations below these levels except for one sample for Pb (K4) and another sample for Zn (K3). Analysis of host dolomitic limestones returned SiO_2 values of 7.57–8.09 wt.%, whereas limestones have relatively lower SiO_2 contents. However, only one sample has higher SiO_2 composition (with 44.99 wt.%), and the limestones usually have high CaO concentrations. Samples K5 and K6 have high MgO contents (Tables 3–4).

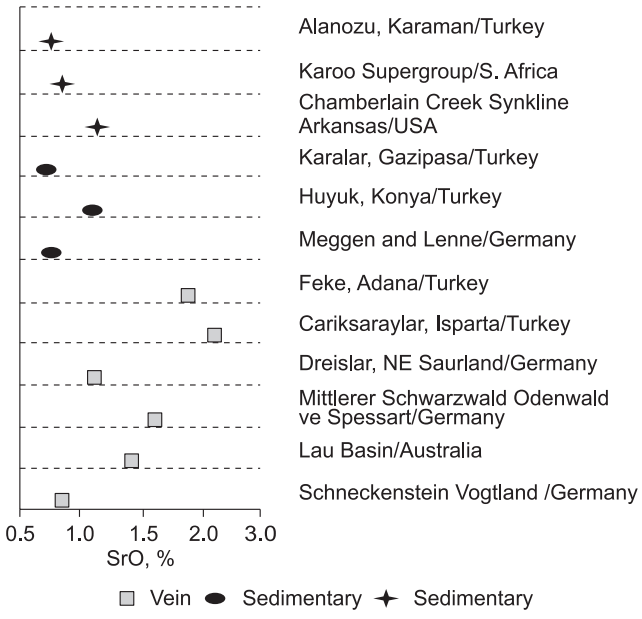

Fig. 5. Several deposit types of barite, percentage of strontium oxide amounts (Kayabalı, 1992; Bertine and Tick, 1975; Fazakas, 1976; Podufal, 1977; Cengiz, 2002; Puchelt, 1967; Ayhan, 1987; Zimmerman, 1976; Reimer, 1978; Striebel, 1965).

5.1.1. Rare earth element geochemistry

The barite samples have low rare earth element presences(Tables 5 and 6). Since the normalized rare earth element values of the barite and host rock samples are close to each other, average values were calculated and plotted on the diagrams. When plotted on

Table 3. **Major element contents of the host rock (in percentage)**

Host Rocks	Sample	BaO	SrO	SiO_2	Al_2O_3	Fe_2O_3	MgO	CaO	Na_2O	K_2O	MnO	LOI
Limestone	K2	1.88	0.08	0.34	<.01	0.36	0.52	55.27	0.02	<.01	0.21	40.9
	K3	0.29	0.84	3.73	1.35	0.46	0.17	19.3	<.01	0.4	0.01	15.3
	K4	0.25	0.07	1.88	0.03	0.53	0.14	28.82	<01	0.02	0.16	21
	K7	0.19	0.08	0.32	<.01	0.42	0.5	60.12	0.02	<.01	0.2	35.1
	K8	0.21	0.09	1.5	<.01	0.37	0.7	58.3	0.01	<.01	0.01	33.5
	K9	0.14	0.11	0.4	<.01	0.3	0.4	50.4	0.01	<.01	0.2	41.4
	K10	0.15	0.41	2.8	1.32	0.32	0.9	48.17	<.01	<.01	0.22	38.6
	K11	0.17	0.29	1.6	0.02	0.4	0.5	56.8	0.02	<.01	0.01	34.8
	K12	0.13	0.03	1.76	0.03	0.44	0.24	46.7	<.01	<.01	0.2	36.9
	K13	0.2	0.08	4.45	1.4	0.48	0.65	59.9	0.03	<.01	0.2	42.3
	K14	0.18	0.08	3.9	1.39	1.73	0.26	53.6	0.02	<.01	0.24	39.9
	K15	0.22	0.07	6.2	1.51	1.6	0.32	43.7	<.01	<.01	0.27	41.9
Dolomitic Limestone	K5	0.19	0.03	7.57	1.63	2.17	10.16	36.98	0.03	0.65	0.39	39.5
	K6	0.2	0.09	8.09	0.01	2.72	8.87	30.68	0.01	<.01	0.49	32.9
Shale	K1	0.49	0.03	44.99	11.17	1.84	1.01	18.97	1.02	3.58	0.06	16.3

Table 4. **Trace element contents of the host rock (ppm)**

Host Rocks	Sample	Ba	Sr	Ni	Co	Ga	Hf	Nb	Rb	Ta	U	Zr	Y	Cu	Pb	Zn	As
Limestone	K2	16842	694	24	1	<.5	<.1	0.1	<.1	0.2	<.1	0.2	12.8	0.7	3.7	3	1.4
	K3	2573	7122	<20	1.1	1.2	1	1.2	14	0.6	0.3	16	2.1	1.7	3.2	39	1
	K4	2246	568	<20	1.1	<.5	0	<.1	0.9	0.7	0.1	0.2	8.9	8.5	36	6	2.9
	K7	1671	654	<20	2.3	<.5	1	0.1	5.5	0.2	<.1	0.2	11.2	0.7	3.5	2	1.5
	K8	1864	783	<20	2.6	1.1	1	1.1	3.4	0.5	<.1	0.3	9.8	4.4	3.9	3	1.4
	K9	1234	892	25	1.2	<.5	0	0.9	0.5	0.4	0.2	0.2	13.1	3.2	6.7	2	1.7
	K10	1345	3452	<20	1.8	<.5	1	0.6	0.8	0.3	<.1	0.5	12.4	0.9	4.2	3	2.1
	K11	1568	2456	<20	1.1	1.1	1	<.1	0.3	0.3	<.1	0.4	11.6	1.2	3.4	4	2.3
	K12	1149	279	32	1	<.5	0	<.1	0.1	0.2	0.4	0.2	12.9	1.6	3.5	3	2.8
	K13	1782	672	36	2.5	<.5	1	0.3	<.1	0.4	<.1	0.3	10.7	0.6	5.1	3	1.9
	K14	1653	655	<20	2.1	<.5	0	0.2	<.1	0.4	0.3	0.2	12.1	0.7	3.2	3	1.4
	K15	1982	598	<20	3.4	0.9	1	<.1	<.1	0.2	<.1	0.2	12.6	0.9	4.1	5	1.5
Dolomitic Limestone	K5	1666	245	<20	2.6	2.3	2	2	21	0.2	0.5	55	8.5	5.6	6	47	0.6
	K6	1789	782	<20	2.2	0.6	0	<.1	0.1	0.8	0.2	0.5	1.4	0.4	7.3	46	1.3
Shale	K1	4423	223	54	18	15	4	14	119	1	1.6	158	19.4	3.7	1.5	1	2.7

a normalized diagram, all analyzed samples displayed similar patterns with characteristic positive Eu anomalies. Rare earth element analyses toward the studied barites have low Ce/Yb values. High Ce/Yb values indicate light rare earth element enrichment in the samples, whereas low Ce/Yb values suggest enrichments in high rare earth elements. In the normalized rare earth element diagrams (Figure 6), positive peaks in La, Dy, and Tm, and relatively low values for the remaining elements resulted in a zigzag pattern.

Chondrite-normalized rare earth element presence plots of hydrothermal minerals are characterized by typical saw-tooth patterns (Ronov et al., 1967). Studied barites have a similar zigzag pattern instead of a smooth pattern. Ce/Ce* and Eu/Eu* ratios (Table 5) are important indicators of oxygen conditions in the environment.

The chondrite-normalized plots (Evensen, 1978) together with Ce/Ce* and Eu/Eu* diagrams (Figure 5) exhibit negative Ce and positive Eu anomalies in barites. Although the studied samples exhibit positive Eu anomalies, presences of other rare earth elements are significantly low. Y is relatively more present in the samples compared to Ce possibly due to the influence of exterior factors on barite crystallization such as faulting. Host rocks are relatively more enriched in rare earth elements relative to the barite samples. Their Ce/Yb ratios show that the host rocks are more enriched in light rare earth elements with respect to barites. Similar to the barites, the limestones and dolomitic limestones also exhibit positive Eu and negative Ce anomalies, suggesting oxidizing conditions. Based on the comparison between the normalized rare earth element compositions of the host rocks, sample K1 has the highest value followed by the limestones and the dolomitic limestones,

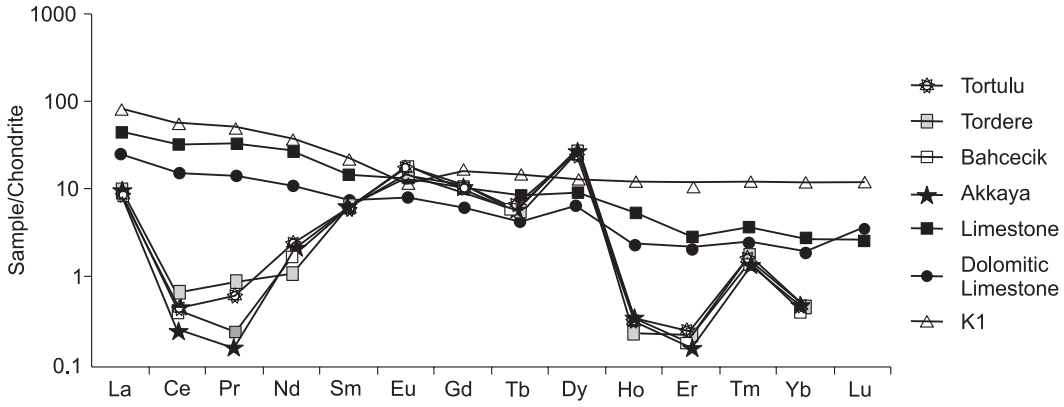

Fig. 6. Chondrite-normalized rare earth element patterns of the host rock and ore samples collected from the study area.

respectively. The C1 chondrite-normalized (after Evensen et al., 1978) rare earth element concentrations of the studied barites and host rocks as well as the concentrations of similar samples, as compiled from the literature, are provided in Figure 7.

Investigation toward the rare earth element compositions of barite samples from various marine and continental settings suggests high rare earth element presences, but minimum chondrite-normalized Eu values for deep marine barite samples. These deep marine barite samples also lack Ce anomalies, which is common in seawaters. The studied barite samples are different from seawater as they exhibit positive Eu anomalies, and although they have lower rare earth element presences related to hydrothermal samples, the rare earth element distributions of the studied barites and the hydrothermal samples are broadly similar. Rare earth element patterns of the hydrothermal samples near the East Pacific Rise (Michard and Albarede, 1986) and the hydrothermal vents from the Salton Sea are characterized by positive Eu anomalies. The hydrothermal fluids of both the Salton Sea and the East Pacific Rise areas are enriched in rare earth elements relative to seawater. Although the

Table 5. **REE contents of the studied barites (ppm)**

Mineral Deposits	Sample	La	Ce	Pr	Nd	Sm	Eu	Gd	Tb	Dy	Ho	Er	Tm	Yb	Lu	Y	Ce/Yb	Ce/Ce*	Eu/ Eu*
Tortulu	T-B1	2.6	0.3	0.03	<.3	0.71	<.02	1.71	0.17	5.92	0.02	<.03	0.04	<.05	<.01	1.2	—	0.2	—
	T-B2	2.2	0.1	<.02	<.3	0.91	<.02	2.27	0.18	6.95	<.02	<.03	0.04	0.07	<.01	1.4	1.43	—	—
	T-B3	2.4	0.1	0.03	<.3	1.05	<.02	2.56	0.2	7.91	<.02	0.03	0.06	0.07	<.01	1.5	1.43	0.08	—
	T-B4	2.3	0.5	0.07	<.3	0.94	<.02	2.3	0.17	6.86	<.02	0.04	0.04	0.07	<.01	1.5	7.14	0.2	—
	T-B5	2.8	0.2	0.03	<.3	1.11	1.05	2.71	0.21	8.39	<.02	0.03	0.05	0.07	<.01	1.6	2.86	0.1	1.8
	T-B6	2.6	0.6	0.13	1.1	1.08	<0.02	2.62	0.2	7.04	<.02	0.06	0.05	0.08	<.01	2.3	7.5	0.2	—
Tordere	TD-B7	2.3	0.4	0.05	<.3	0.87	0.73	2.06	0.15	6.13	<.02	0.03	0.03	0.06	<.01	1.3	4.29	0.2	1.6
	TD-B8	2.1	0.2	0.03	<.3	0.9	<.02	2.52	0.14	6.24	<.02	0.03	0.04	0.07	<.01	1.2	6.67	0.1	—
	TD-B9	2.3	0.1	0.01	<.3	1.02	<.02	2.15	0.23	7.45	<.02	0.04	0.05	0.08	<.01	1.3	2.86	0.1	—
	TD-B10	3.1	0.7	0.07	0.4	1.24	0.76	2.88	0.21	8.61	<.02	0.04	0.06	0.09	<.01	1.7	1.25	0.3	1.4
	TD-B11	2.4	0.4	0.03	0.4	0.93	0.74	2.48	0.27	6.8	0.01	0.03	0.04	0.08	<.01	2.2	7.78	0.3	1.8
	TD-B12	2.2	0.3	0.05	0.5	0.98	1.02	2.3	0.18	7.4	0.02	<.03	0.05	0.07	<.01	1.7	5	0.2	1.8
	TD-B13	3.1	1.2	0.21	0.8	1.09	1.07	2.56	0.2	7.38	<.02	<.03	0.05	0.09	<.01	1.35	4.29	0.3	2.1
	TD-B14	2.7	0.1	0.23	<.3	0.81	0.76	2.48	0.24	6.98	0.01	0.03	0.06	0.07	<.01	1.6	13.33	0.03	1.6
Bahcecik	B-B15	2.3	0.3	0.03	<.3	1.13	1.01	1.94	0.2	6.67	0.02	0.03	0.03	0.08	<.01	1.43	1.43	0.09	1.6
	B-B16	2.6	0.3	0.03	0.8	0.96	1.07	2.84	0.19	8.2	0.02	<.03	0.04	0.05	<.01	1.42	5	0.2	1.8
	B-B17	2.3	0.2	0.01	<.3	0.91	0.76	2.66	0.16	6.1	0.02	0.03	0.03	0.07	<.01	1.65	3.75	—	1.7
Akkaya	A-B18	2.4	0.1	0.02	0.9	0.9	0.78	2.36	0.18	6.64	<.02	0.02	0.04	0.06	<.01	1.2	6	0.1	1.7
	A-B19	2.2	0.1	<.02	<.3	0.89	<.02	2.91	0.17	7.01	0.02	<.03	0.04	0.08	<.01	1.5	2.86	—	—
	A-B20	2.6	0.3	0.01	<.3	1.05	<.02	2.04	0.21	7.6	0.02	0.03	0.03	0.07	<.01	1.7	4.29	0.4	—

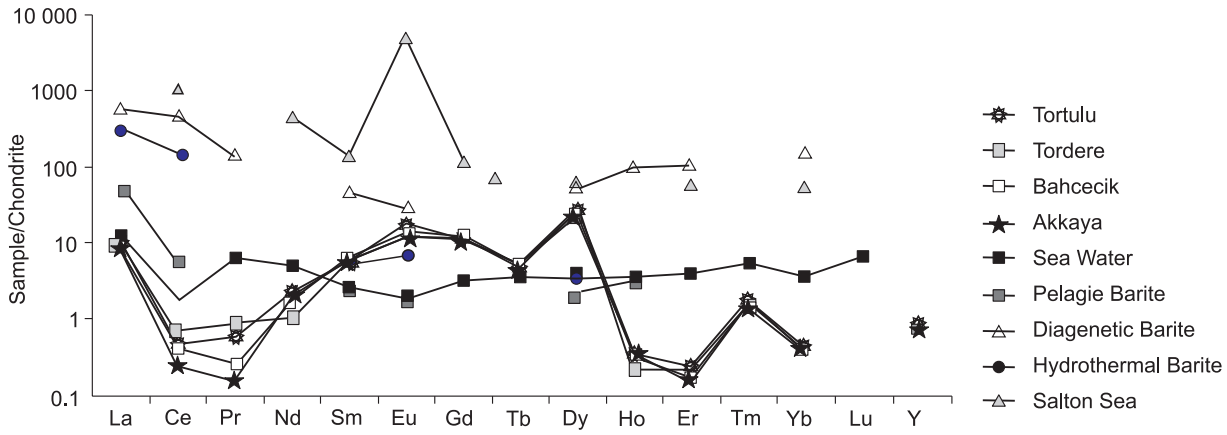

Fig. 7. Plot showing comparisons between chondrite-normalized rare earth element compositions of the studied barite samples and various other barite occurrences.

studied barites have broadly similar compositions with that of the Salton Sea fluids, the barites have relatively higher rare earth element presences. When compared to other barite samples, barites from the study area are somewhat similar to the hydrothermal barite sample CB3. When plotted on $Ce_N/ Yb_N – Yb_N$ and Ce_N/Sm_N - Ce_N/Yb_N diagrams together with several other hydrothermal systems and barite deposits from around the world, barite samples fall near the field defined by seawaters (Table 7, Figures 8–9). Based on this diagram, it can be suggested that the barites were formed from marine hydrothermal fluids, which were enriched in elements through leaching out of the host rocks.

Table 6. **REE contents of the studied host rocks (ppm)**

Host Rocks	Sample	La	Ce	Pr	Nd	Sm	Eu	Gd	Tb	Dy	Ho	Er	Tm	Yb	Lu	Ce/Yb
Limestone	K2	13.4	29	4.05	16	2.74	0.24	2.7	0.37	2.06	0.33	0.77	0.1	0.5	0.06	58
	K3	5.1	3.8	0.51	1.9	0.68	1.12	1.24	0.1	1.52	0.05	0.13	0.04	0.15	0.03	25.33
	K4	5.8	11	1.46	6.6	2.15	1.7	2.64	0.26	2.75	0.17	0.41	0.07	0.32	0.05	34.38
	K7	14.2	25	4.16	13	2.4	0.34	2.6	0.43	2.8	0.35	0.78	0.1	0.25	0.03	100
	K8	12.4	26	4.25	17	2.8	0.8	1.7	0.1	2.67	0.32	0.16	0.3	0.3	0.04	86.67
	K9	11.5	22	3.87	16	2.91	0.45	1.5	0.06	1.96	0.56	0.32	0.01	0.6	0.05	36.67
	K10	13.1	20	2.9	18	2.27	0.37	2.9	0.52	2.34	0.25	0.45	0.06	0.6	0.06	33.33
	K11	14	18	3.56	16	2.34	0.97	2.7	0.5	3.15	0.15	0.64	0.07	0.5	0.3	36
	K12	13.8	30	4.67	15	2.86	0.32	1.89	0.47	2.56	0.25	0.08	0.02	0.39	0.06	76.92
	K13	8.9	20	3.4	16	1.98	0.28	1.75	0.1	1.85	0.4	0.07	0.37	0.2	0.08	100
	K14	10.8	25	2.97	11	2.3	1.1	1.9	0.4	2.89	0.36	0.71	0.04	1.4	0.07	17.86
	K15	12.7	27	3.7	15	2.56	1.5	2.4	0.49	2.13	0.52	1.55	0.02	0.5	0.03	54
Dolomitic Limestone	K5	11.1	18	2.45	9.5	1.79	0.43	1.67	0.24	1.22	0.24	0.65	0.11	0.6	0.09	30
	K6	1.4	1.5	0.24	1.1	0.49	0.51	0.9	0.07	2.05	0.03	0.07	0.02	0.06	<.01	25
Quartzite	K1	20	36	4.86	18	3.48	0.68	3.26	0.54	3.23	0.68	1.93	0.32	1.95	0.3	18.46

Table 7. **Ce_N/ Yb_N-Yb_N — Ce_N/Sm_N — Ce_N/Yb_N contents of the average of the studied barites**

	Ce_N/Yb_N	Yb_N	Ce_N/Sm_N	Ce_N/Yb_N
Tortulu	1.08	0.44	0.07	1.08
Tordere	1.23	0.46	0.09	1.23
Bahcecik	1.03	0.4	0.06	1.03
Akkaya	0.62	0.42	0.04	0.62
Limestone	11.5	2.88	2.19	11.5
Dolomitic	7.48	2	2.02	7.48
K1	4.79	11.82	2.5	4.79
Sea Water	0.49	3.82	0.67	0.49
Diagenetic Barite	3.07	157.58	10.08	3.07
Salton Sea	19.57	56.55	7.54	19.57

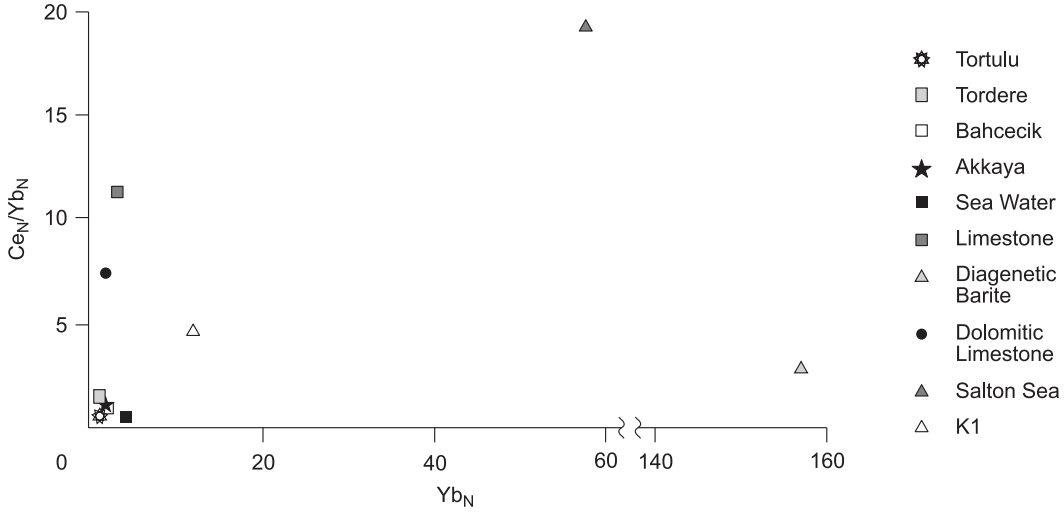

Fig. 8. Plot of normalized Ce_N/Yb_N versus Yb_N for the rock and barite samples collected from the study area.

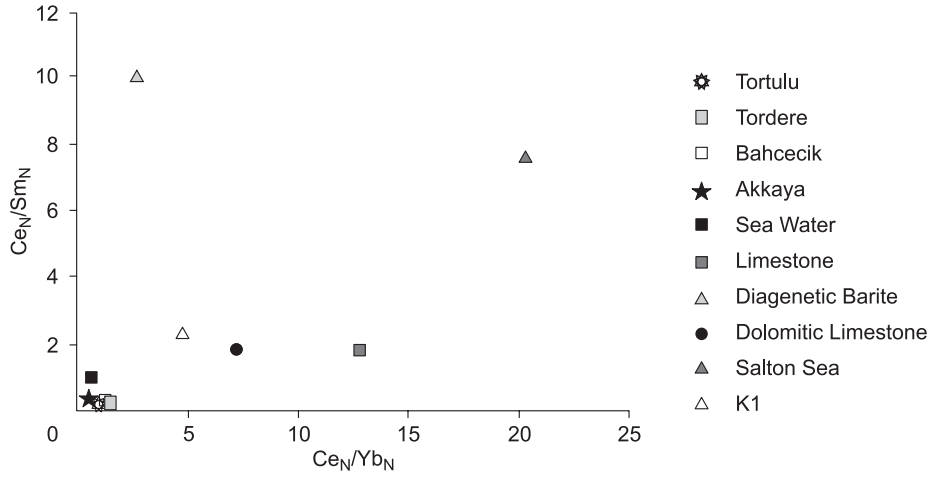

Fig. 9. Plot of normalized Ce_N/Sm_N versus Ce_N/Yb_N for the rock and barite samples collected from the study.

5.2. Fluid inclusion data

Fluid inclusion samples B-1 and B-4 were collected from Tortulu area, whereas samples B10, B8, and B7 were obtained from the Tordere area. Fluid inclusions of primary and secondary origin were observed in both mineral phases. Majority of the primary inclusions are single-phase (L) inclusions, whereas two-phase (L+V) inclusions are rare in the samples. On the other hand, secondary inclusions are single-phase (L) inclusions that locally show evidence of necking down. Most of the measurements were taken from the two-phase (L+V) primary inclusions. A total of 6 microthermometric measurements recorded from the barite crystals in sample B1 indicated a range of homogenization temperatures (Th°C) between 78 and 187°C (Figure 10).

Due to the coexistence of single-phase aqueous and single-phase vapor-filled inclusions, the recorded homogenization temperatures were directly considered as the temperature of formation. Fluid inclusions were frozen using liquid nitrogen, and melting temperatures (Tm °C) could be measured on only 2 inclusions. These inclusions yielded melting temperatures of -0.5 and -0.9°C. Salinity values calculated (as NaCl wt.% equivalent) from these melting temperatures utilizing the equation of Bodnar (1993) are 0.9 and 1.6 wt.% NaCl equivalent, respectively, and these values are considered to represent the salinity range of the fluids. In sample B4, analyzed single-phase inclusions (L) have sizes ranging between 2 and 18 microns with most inclusions falling into the range of 2–8 microns. Two-phase (L+V) inclusions, on the other hand, have sizes ranging between 2–10 microns. Similarly, sizes of the two-phase (L+V) fluid inclusions in sample B10 are between 2–10

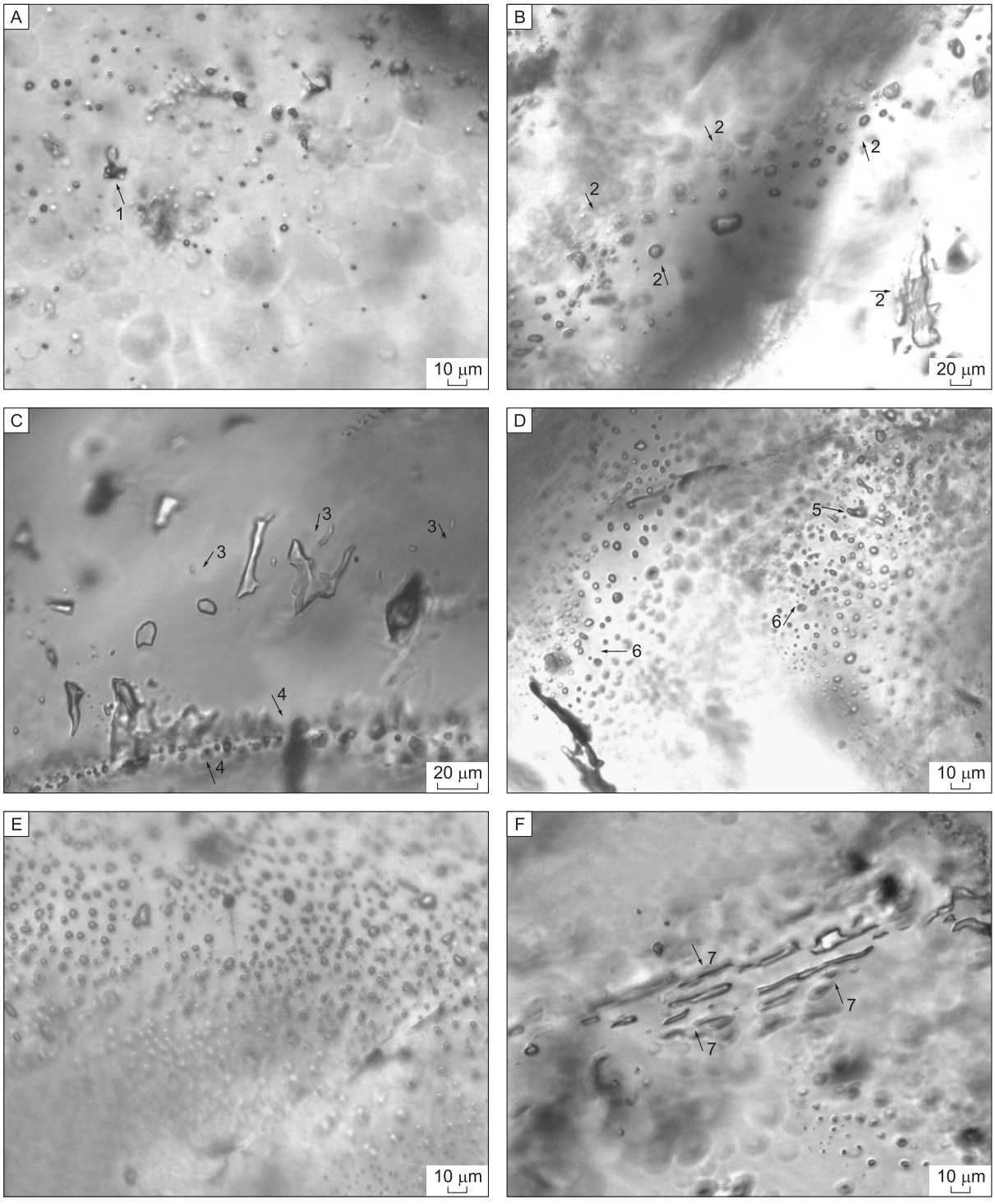

Fig. 10. Photomicrographs showing fluid inclusion types observed in this study.
A. 1:Two-phase (L+V) fluid inclusion in barite. B. 2:Single-phase fluid inclusion in the B1 barite sample. C. 3: Primary single-phase fluid inclusion in the B4 barite sample, 4: Secondary single-phase fluid inclusion in the B4 barite sample. D. Fluid inclusions in the B10 barite sample. 5: Two-phase (liquid+gas) inclusions, 6: Single phase (liquid) inclusions. E. Single-phase (L) fluid inclusion in the B10 barite sample. Crystal plane of the observed single-phase inclusions. F. Necked and stretched single-phase fluid inclusion in the barite sample B7. 7: Necked and stretched single-phase (liquid) inclusions of secondary origin.

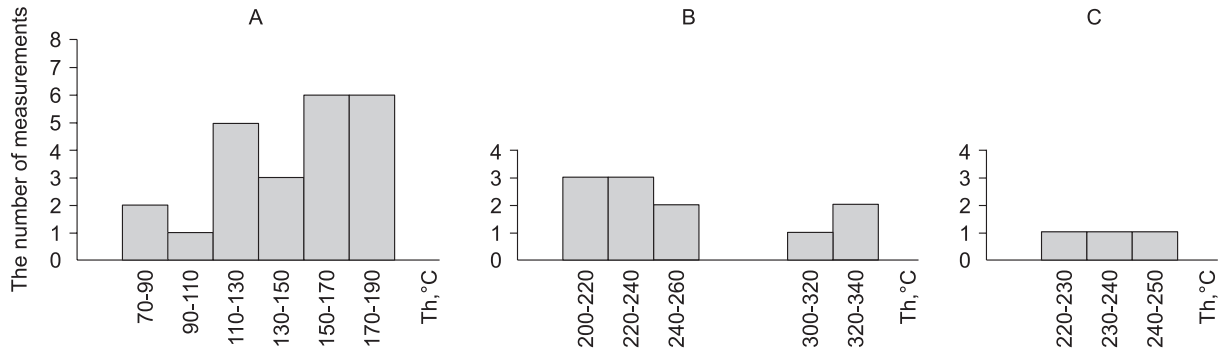

Fig. 11. Diagrams showing homogenization temperatures of the studied fluid inclusions in A. barite, B. quartz, and C. calcite.

microns. Microthermometric measurements conducted on three of the primary two-phase (L+V) fluid inclusions hosted by barite crystals in sample B8 yielded homogenization temperatures of 114, 143, and 170°C. The presence of two-phase (L+V) fluid inclusions in sample B7 is quite scarce, and the observed inclusions have sizes varying between 2–12 microns with majority of inclusions having sizes of 2–8 microns. Secondary single-phase fluid inclusions in this sample are usually between 2–10 microns in size, but some of the inclusion sizes may reach up to 20 microns. Quartz crystals in the samples were also analyzed. (Figure 11).

The inclusion was frozen using liquid nitrogen and upon heating a melting temperature (Tm°C) of -1.3°C was obtained. Therefore, it can be suggested that quartz was precipitated from low salinity hydrothermal fluids which were probably diluted upon mixing with meteoric waters. The homogenization temperatures measured from inclusions hosted by calcite crystals are 221, 233, and 249°C, indicating a range of 221–249°C for homogenization temperatures as shown on the histogram in Figure 11. In addition, alignments of relatively small-sized, paragenetically late one- and two-phase secondary inclusions were identified within barite crystals. However, no microthermometric analyses were performed on these inclusions since they are unimportant as far as the formation temperature of the barites is concerned. As one- and two-phase inclusions coexist in the samples, the measured homogenization temperatures are directly regarded as the formation temperatures. They are also plotted on a diagram in Figure 11. A total of 23 microthermometric measurements on barite crystals indicate homogenization temperatures of between 78 and 190°C with majority of data grouping between 150 and 190°C. Accordingly, the barite crystallization began around 190°C and continued until 70–90°C. Melting temperatures (Tm°C) obtained from freezing runs yielded salinity values of 0.9, 1.2, 1.4, and 1.6 wt.% NaCl equivalent indicating a salinity range of 0.9–1.6 wt.% NaCl equivalent. This suggests that the barite crystals were formed from low salinity hydrothermal solutions, which were further diluted possibly upon mixing with meteoric waters. Barite formation likely corresponds to the epithermal stage of the hydrothermal system. Hydrothermal minerals consist of fluid inclusions containing two or three of the vapor, liquid, and solid phases, but mostly in the form of a liquid phase enclosing a vapor bubble. As a result, quartz was formed initially from the hydrothermal solutions followed by precipitation of calcite and barite, respectively. The low homogenization temperatures suggest that barite was formed at a late stage, whereas quartz and calcite were formed at relatively higher temperatures. Upon their presence, the temperatures of the hydrothermal solutions decreased, but their salinity values remained the same. It is possible that they were mixed with meteoric fluids at shallow depths. Homogenization temperatures measured from primary fluid inclusions indicate that the barite deposits are of hydrothermal origin, and they were probably formed during epithermal-mesothermal stages of the hydrothermal system. It is very important for some Russian researchers who elaborated methods and instruments for studying fluid inclusions in minerals, including those from low-temperature (epithermal) deposits of this type. The compressibility of 20 % NaCl solution, at 150 °C, is so small that even 3,300 m of hydrostatic head on it would only cause a pressure correction of 25° (Klevtsov and Lemmlein, 1959). Sourirajon and Kennedy (1962) show that 25 weight percent NaCl raises the critical point for water to about 670^{0}C, and many critical point determinations on fluid inclusions fall in the range pf 375° to 450 °C (Dolgov, YU. A , Bazarov L,Sh, Bakumenko I.T. 1968)

5.3. Isotopic analysis

5.3.1. Strontium isotope results of barites

A summary of the **s**trontium isotope compositions of the barite samples (Tortulu, Tordere, Bahcecik and Akkaya) collected from the study area as well as the analyzed mineral phases and other relevant properties are provided in Table 8 and Figure 12 [standard NBS 987 ^{87}Sr / ^{86}Sr 0,710240 +/- 0,000014 (2σ)].

Table 8. **Deposition style, host rock, and mineralogy of barites $^{87}Sr/^{86}Sr$. ^{34}S isotope results**

Mineral Deposits	Sample	Host Rock	Deposition Style	Mineralogy	$^{87}Sr/^{86}Sr$	^{34}S ‰ (CDT)
Tortulu	B1	Limestone	Vein	Barite	0.709898	33.9
Tortulu	B4	Limestone	Vein	Barite	0.707783	35.3
Tortulu	B5	Limestone	Vein	Barite	0.706432	34.1
Tordere	B10	Limestone	Vein	Barite	0.749652	32.2
Tordere	B11	Limestone	Vein	Barite	0.710323	32.8
Tordere	B8	Limestone	Vein	Barite	0.700211	36.8
Bahcecik	B17	Limestone	Vein	Barite	0.710312	34.3
Akkaya	B20	Limestone	Vein	Barite	0.709885	33.7

Barites collected from the study area have $^{87}Sr/^{86}Sr$ values that are higher than the values obtained from the marine carbonates of Infracambrian Period (Figure 12).

These values were also compared to the Sr isotopic compositions of similar deposits (Figure 13). The Sr values obtained from the barite, metabasalt, and dolomite samples from the Calabria and Sardinia deposits in Italy have Sr contents between 0.6 and 3.2%. The low values correspond to the synsedimentary barites, whereas higher Sr values are associated with remobilized barites. Karstic barites from Sardinia and Calabria have $^{87}Sr/^{86}Sr$ values of 0.70947 and 0.7073–0.70710, respectively (Barbieri et al., 1984) (Figure 13).

$^{87}Sr/^{86}Sr$ values can be used for barites since the Ba-Sr solid solution series of $BaSO_4$–$SrSO_4$ and layers do not contain any Rb. Stratiform marine barite deposits have lower $^{87}Sr/^{86}Sr$ values compared to Sardinia and Calabria. However, hydrothermal barite deposits have $^{87}Sr/^{86}Sr$ values that are higher than 0.71. The hydrothermal barite deposits in Sierra de Guadarrama (Spain) have $^{87}Sr/^{86}Sr$ values ranging between 0.715567 and 0.717164 (Galindo et al., 1994). Precambrian schists have $^{87}Sr/^{86}Sr$ values between 0.712 and 0.730 (Holland, 1984). The $^{87}Sr/^{86}Sr$ value of the Aravalli barite deposit is 0.7234, and these deposits were suggested to have formed from continental rocks (Deb et al., 1991). In the Tons Valley, the barites are characterized by $^{87}Sr/^{86}Sr$ values of 0.7204–0.7286. The barites at Tons Valley are relevant old continental rocks, and magmatic or marine volcanic activity was not effective for their formation. Fluids derived through the recrystallization of the Proterozoic parent rocks were suggested to be responsible for the formation of these barites (Sharma et al., 2003). The high $^{87}Sr/^{86}Sr$ values observed in the studied samples (0.749652; sample B10) is indicative of mineralization via remobilization and a continental origin. Barites in the region may have formed from pre-Paleozoic shallow marine rocks. In addition to that, contribution from seawater Sr is another possibility for the formation of the barites. According to the strontium isotopic analysis, the source of the Sr that is found within the barites in the study area is probably the hydrothermal fluids that were possibly derived from a buried intrusion, which is later interacted with the pre-Paleozoic basement rocks and then mixed with waters of meteoric or seawater

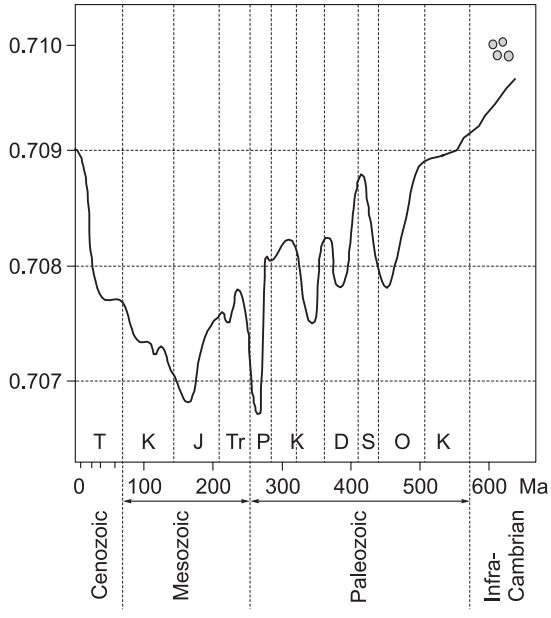

Fig. 12. $^{87}Sr/^{86}Sr$ values of Phanerozoic marine carbonates (Faure, 1977).

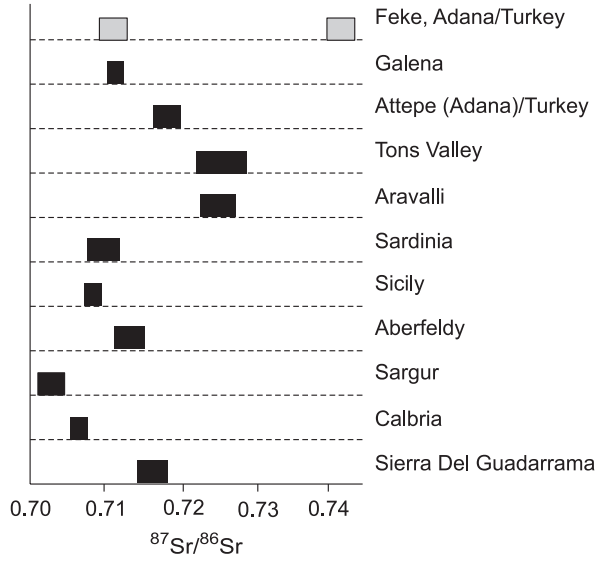

Fig. 13. $^{87}Sr/^{86}Sr$ values from the study area and other barite deposits.

origin. With the exception of one sample (B10), the $^{87}Sr/^{86}Sr$ values of the studied barites are consistent with hydrothermally-formed barites.

5.3.2. Sulfur isotope results of barites

A summary of the sulfur isotope compositions of the barite samples collected from the study area as well as the analyzed mineral phases and other relevant properties are provided in Table 8. Seawater is an important sulfur reservoir with its high SO_4^- concentrations. The sulfur isotopic composition of seawater has varied in geological time with $\delta^{34}S$ between +10 and +30‰, and in modern seawater it has a value between +17 and +20‰ (Claypool et al., 1980; Ohmoto, 1986) (Figure 14).

During the Paleozoic Era, the $\delta^{34}S$ values of seawater were between +15 and +35‰ (Faure, 1986; Hanor, 2000), whereas the maximum $\delta^{34}S$ values for seawater sulfate during the Cambrian-Ordovician period (about 550–450 m years ago) were between +25 and +35‰. These values are similar to those of the barites analyzed in this study, with the exception of two samples (B4 and B8). Studies on hydrothermal deposits revealed highly complex results, which were interpreted either as mixing of different sulfur reservoirs or as complexities due to physicochemical conditions of the hydrothermal systems (Figure 15).

$\delta^{34}S$ isotope analyses of barite samples collected from the study area yielded $\delta^{34}S$ values between 32.2 and 36.3‰. These values are significantly higher than the sulfur isotopic composition of the seawater SO_4^{--} (average of +20‰). A difference of up to +2‰, relative to seawater values, can be observed in sulfate minerals. These high $\delta^{34}S$ values (samples B4 and B8) indicate that the isotopic compositions were significantly fractionated and enriched in $\delta^{34}S$ relative to seawater. Hydrothermally-derived barites from the Sierra De Guadarrama deposit have $\delta^{34}S$ values around +15‰ (Galindo et al., 1994); Aravalli barite deposits derived from continental rocks have $\delta^{34}S$ values between +17 and +21‰ (Deb et al., 1991); Aberfeldy barites have $\delta^{34}S$ values of +40‰ (Hall et al., 1991), and the barites from the Tons Valley have $\delta^{34}S$ values in the range of +26.4 – +29.5‰ (Sharma et al., 2003) (Figure 16).

The Peru Margin seawater, which is of biogenic origin, has very high $\delta^{34}S$ values of around +50.6‰ due to the enhanced bacterial reduction (Paytan et al., 2002). On the other hand, karstic barites from Sardinia have $\delta^{34}S$ values varying between +14 and 21.9‰ (Barbieri et al., 1984), whereas barites from the Gulf of Mexico have $\delta^{34}S$ compositions of +28.5 and +59.5‰ (Fu and Aharon, 1997). A comparison between the $^{87}Sr/^{86}Sr$ and $\delta^{34}S$ compositions of the studied barites and the other barite deposits from elsewhere around the world suggests similarities to the Peru Margin and the Gulf of Mexico with high $\delta^{34}S$ and low $^{87}Sr/^{86}Sr$ compositions (Figure 16). When compared against various barite deposits from around the world, studied barites display similarities to the Mississippi Valley-type deposits in terms of sulfur isotopic compositions (Figure 17).

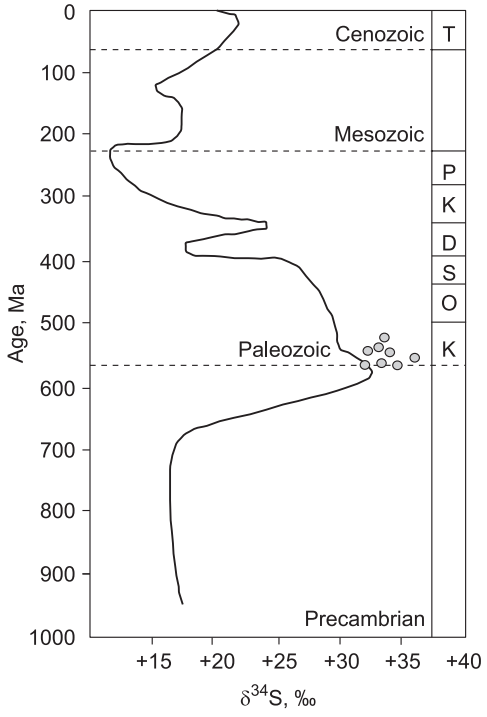

Fig. 14 $\delta^{34}S$ values of marine sulfate minerals from Precambrian to Recent time (Faure, 1986).

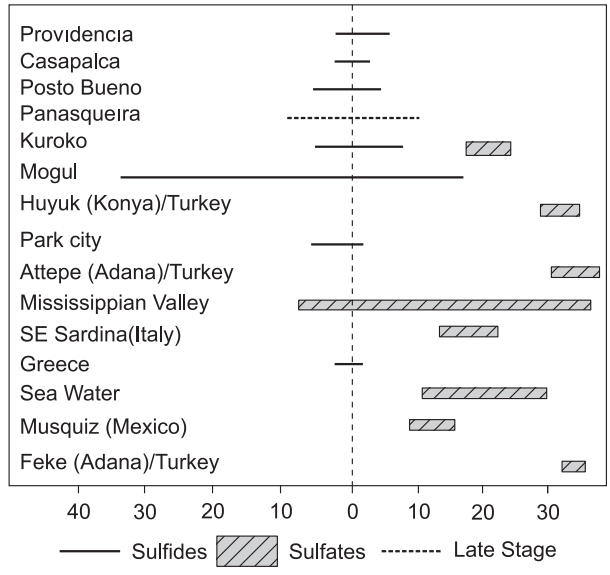

Fig. 15. $\delta^{34}S$ values of sulfide and sulfate minerals from various geologic settings and ore deposits (Rye and Ohmoto, 1974; Ohmoto and Rye, 1979; Cengiz and Kuscu, 2002; Küpeli et al., 2006; Barbieri et al., 1984; Kesler and Jones, 1981).

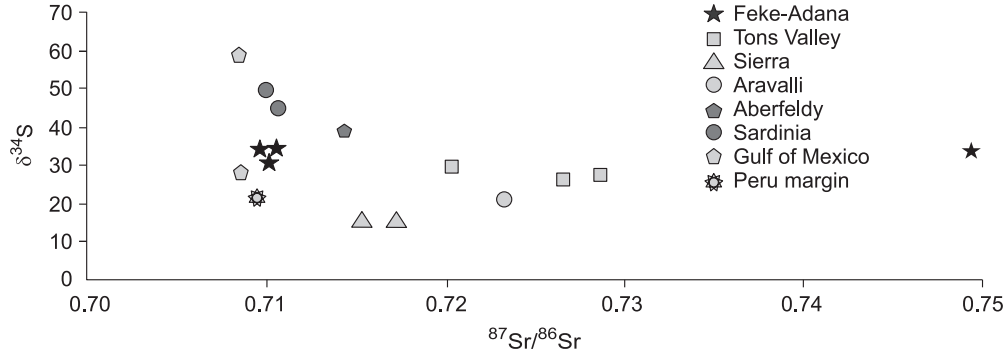

Fig. 16. Comparison diagram of $^{87}Sr/^{86}Sr$-$\delta^{34}S$ between the Feke-Adana barite deposits and various barite deposits from the world.

Deposits such as Punta Peppixedda, Monte Tasua, Huyuk and Konya are examples of Mississippi Valley-type deposits, and they have $\delta^{34}S$ isotopic compositions between +30.15 and +32.1‰. Therefore, studied barites have positive $\delta^{34}S$ values close to +37‰.

6. DISCUSSION

Barite deposits within the study area are usually found either within the limestone and dolomitic limestone units of the Cambrian Degirmentas Formation or along the contact zones between these two types of stones. Orebodies were formed within the fracture zones and open spaces of these units generally in the form of veins and lodes. In terms of metallogeny, the absence of magmatic rocks in the region and the locations of the orebodies make it difficult to determine the source of barium. Barite deposits are paragenetically uniform. Based on their crystal sizes, two distinct groups of barites were identified within the veins. Coarse-grained barites are locally accompanied by fine-grained barite grains, which surround and hold the clasts of the host rock breccias together in a way similar to the cement material observed in clastic sedimentary rocks. These fine-grained rocks represent a later stage phase. In thin section, observed features such as replacement textures, partitioning, inclusions, and fracture fillings are typical of vein-type samples. Euhedral to subhedral, coarse-grained and locally radiating crystals of barite, which have undergone intense cataclastic deformation, were also often observed in the samples. Such samples of radiating crystals are common in hydrothermal deposits (Ayhan, 1981; Ayhan, 1983; Brodtkorb et al., 1989; Marumo, 1989). The apparent lacking of clastic textures associated with syngenetic deposits is taken as an evidence for an epigenetic origin for the mineralizations following the formation of limestones. The presence of quartz crystals within barites, the presence of iron-rich specularite and other features characterizing high-temperature samples, and the sample of specularite as infillings surrounding the cataclastic fractures all suggest the role of hydrothermal and remobilization processes during formation of the barite veins. In addition, the samples of various hydrothermal alterations such as silicification, limonitization, dolomitization, and ankeritization indicate the hydrothermal character of mineralization. The SrO contents detected in the veins through geochemical analysis are higher than those of ore deposits of sedimentary origin, and the high SrO presences are correlative with hydrothermal deposits (Werner, 1958; Starke, 1969). Ba and Sr contents differ from the range reported from exhalative-sedimentary deposits, and they show abrupt changes when compared to each other. This situation can be explained by remobilization. The hydrothermal solutions, which facilitated barite mineralization, contain two-phase (L+V) fluid inclusions with homogenization temperatures in the range of

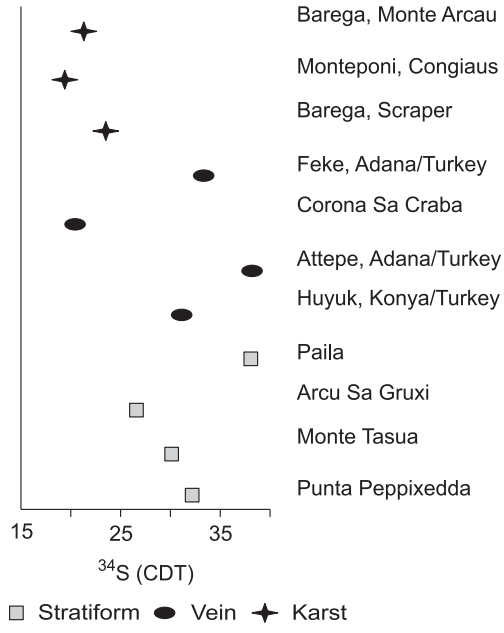

Fig. 17. $\delta^{34}S$ isotope data from the Feke-Adana barite deposits and various other deposits from the world (Barbieri et al., 1984; Kesler and Jones, 1981; Kupeli et al., 2006; Cengiz and Kuscu, 2002).

78–190°C. This, combined with relatively high homogenization temperatures (206–340°C) measured in quartz crystals, also supports that vein-style mineralization was developed during hydrothermal stages. Additionally, low salinities of fluid inclusions indicate interaction with meteoric waters. $^{87}Sr/^{86}Sr$ isotopic compositions, on the other hand, show similarities to hydrothermal samples of continental derivation, indicating that the barite deposition emerged via mixing of hydrothermal solutions. $\delta^{34}S$ isotopic analysis of barites yielded $\delta^{34}S$ values of +32.2–36.3 ‰. The positive $\delta^{34}S$ values are consistent with both sedimentary and hydrothermal deposits. Sulfur, which emerges in hydrothermal deposits within sulfide and/or sulfate minerals, can be either derived from magmatic or seawater sources. It can be suggested that the positive $\delta^{34}S$ values result from the contribution of one of these sources. Another possibility is that the hydrothermal solutions forming the barites may have been mixed with seawater. In the study area, no evidence of magmatic activity and hydrothermal origin forming the deposit was found. The widespread sample of the barite mineralizations within carbonate rocks, their depositional styles, fluid inclusion data, S isotope ratios, and lacking of direct evidence for association with magmatic rocks suggest similarities to the Mississippi Valley-type deposits. The formation of the vein-type ores display similarities to the epigenetic characteristics associated with magmatic activity based on the model developed by Amstutz and Zimmermann (1964). According to this, the ore minerals were transported by magmatic-hydrothermal or regenerative hydrothermal solutions, or by their mixtures. Barites may have formed from such solutions along the fracture zones, or partly from their replacement of the host rocks. In the light of these, the formation of these barite deposits was probably controlled by fault tectonics and hydrothermal activities. Apart from the deeply-derived hydrothermal fluids, the interaction between the meteoric waters and the host basement rocks may have contributed to the enrichment of barium in these solutions, which was possibly remobilized later due to syntectonic movements as well as due to late stage tectonic movements. Barite deposits in the study area are hosted by the Cambrian Degirmentas Limestone. Similar barite samples were also observed in the Ordovician Armutludere Formation. This, combined with the sample of Horzum Pb-Zn mineralizations within Cambrian limestones about 5 km south of the study area indicates a lower age limit of Cambrian or Ordovician Period for the formation of such deposits. However, there is no evidence as of yet for an upper age limit.

7. CONCLUSIONS

The study area comprises, from bottom to top, Infracambrian–Tertiary formations and members identified within these formations. The Neogene and Quaternary deposits stratigraphically lie at the top of the sequence. The oldest rock units in the study area are the Infracambrian units, which have been folded and undergone low-grade greenschist metamorphism following the initial stage of deposition and mineralization.

The NE–SW-oriented barite bodies were epigenetically formed within the limestone and dolomitic limestone levels at the base of the Cambrian Degirmentas Formation, and they are conformable with the fracture systems of the lithostratigraphic unit within which they are hosted. These small-scale fracture systems were generally observed within the limestones and dolomitic limestones, and they provided space for the penetration of the barite-bearing solutions. The barite orebodies, which presumably have undergone metamorphism, generally emerge in the form of veins or lodes.

Mineralogical studies of the orebodies identified in the region are paragenetically uniform consisting of barite, calcite, and quartz, and they typically lack sulfide minerals. Secondary mineral phases, on the other hand, are fluorite, plagioclase (albite), local sericite, and chloritized biotite that appear to be opaque.

Typical XRD diagrams obtained from all samples indicate predominant barite, calcite, and quartz, whereas the main constituents of the host rocks are calcite, quartz, and dolomite. Sparse mica, fluorite, feldspar, and amphibole were also observed in the samples.

Barium is the main element within the barite samples, which typically have low trace element presences. Minor amounts of trace elements such as Pb, Zn, Ni, Co, and As were also identified in the barites. Geochemical analyses indicated SrO presences between 1.02 and 2.28 wt.%. High SrO values of the studied barite samples correlate well with deposits of hydrothermal origin. In addition, elevated Sr contents of the vein-type barites further imply an epigenetic character for the barite mineralizations.

The barites have low rare earth element presences. On a normalized lanthanide diagram, rare earth elements display zigzag patterns with negative Ce and positive Eu anomalies. Negative Ce anomalies indicate conditions of high oxygen fugacity in the source regions of the hydrothermal fluids, whereas positive Eu anomalies show that these conditions prevailed during the stages of ore formation. The latter anomaly also indicates that the mineralizing fluids were formed through alteration of Eu-rich feldspars of dendritic or magmatic origin.

On $Ce_N/Yb_N - Yb_N$ and $Ce_N/Sm_N - Ce_N/Yb_N$ diagrams, analyzed samples cluster in the field for seawater values.

Fluid inclusion analysis revealed that the barite samples are relatively rich in single-phase (L) fluid inclusions compared to two-phase (L+V) fluid inclusions. Single-phase (L) fluid inclusions are either of primary or secondary origin indicating temperature conditions around or below 100°C (or even below 65°C). According to

the microthermometric data obtained from barites, mineralizing fluids have low salinities (0.9-1.6 wt.% NaCl eq.) with homogenization temperatures between 78 and 190°C. On the other hand, homogenization temperatures obtained from quartz fall between 210 and 340°C. Calcite crystals usually contain single-phase (L) inclusions, but measurements obtained from two-phase (L+V) inclusions yielded homogenization temperatures of 221–249°C. Hydrothermal solutions from which quartz and calcite precipitated are also low salinity (2.2 wt.% NaCl eq.) fluids. Homogenization temperatures of the studied primary fluid inclusions suggest a hydrothermal origin for the barite deposits, which were probably formed at epithermal to mesothermal conditions.

$^{87}Sr/^{86}Sr$ isotopic compositions of the barite samples range between 0.709885 and 0.749652. High Sr contents are indicative of remobilization during mineralization and, with the exception of one sample (B10), they correlate well with barites of hydrothermal origin, but not with barites of seawater origin. The $^{87}Sr/^{86}Sr$ isotopic composition of sample B10 is more radiogenic than the other samples.

$\delta^{34}S$ isotopic compositions of the barites collected from the study area range between 32.2 and 36.3‰ (CDT). These values are significantly higher than the isotopic composition of seawater SO_4^-. This indicates that the isotopic composition of the mineralizing environment is significantly differentiated and richer in $\delta^{34}S$ relative to seawater.

The deposition styles, mineral associations, trace element compositions, fluid inclusion data, and the $^{87}Sr/^{86}Sr$ and $\delta^{34}S$ isotopic compositions of barites suggest formation from hydrothermal fluids, which were probably derived from a buried intrusion and mixed with meteoric and marine waters later interacting with the Paleozoic metaclastic and carbonate host rocks.

Acknowledgements

This study was supported with a Scientific Research Support Fund from Cukurova University.

REFERENCES

Amstutz, G.C., Zimmermann, R.A., 1964. Small scale sedimentary features in the Arkansas barite district, in: Amstutz, G.C. (Ed.), Sedimentology and Ore Genesis. Elsevier, Amsterdam, pp. 157–163.

Ayhan, A., 1981. Pb–Zn deposits Aydap Yulari (Gazipasa–Antalya) and the origin of the problem remobilization. MTA 95/96, 101–112.

Ayhan, A., 1983. In the eastern Taurus Mountains, Cambrian–Ordovician sedimentary sequence and propagation. Bull. Geol. Soc. Turk. 4, 17–20.

Ayhan, A., 1987. Huyuk (Konya) and Sarkikaraagac (Isparta): Investigation of Barite Deposits Located Between. SU. Research Fund Report No. 45.

Ayhan, A., 1988. Turkey Geological Map Series, Kozan-J 21 Layout [in Turkey]. MTA Report No. 12, Ankara.

Barbieri, M., Vivo, B., Perrone, V., Turco, E., 1984a. Strontium geochemistry of the San Donato barite mineralization. Chem. Geol. 45, 279–288.

Barbieri, M., Masi, U., Tolomio, L., 1984b. Strontium geochemical evidence for the origin of the barite deposits from Sardinia (Italy). Econom. Geol. 79, 1360–1365.

Bertine, K.K., Keene, J.B., 1975. Submarine barite–opal rocks of hydrothermal origin. Science 188, 150–152.

Bodnar, R.J., 1993. Revised equation and table for determining the freezing point depression of H_2O–NaCl solutions. Geochim. Cosmochim. Acta 57, 683–684.

Brodtkorb, M.K., Schalamuk, I.B.A., Ametrano, S., 1989. Barite and celestite stratabound ore fields in Argentina, in: De Brodtkorb, M.K. (Ed.), Non-Metalliferous Stratabound Ore Fields. Van Nostrand Reinhold, New York, pp. 41–68.

Cengiz, O., Kuscu, M., 2002. Geochemical characteristics and origin of barite deposit between Sarkikaraagac (Isparta) and Huyuk (Konya) [in Turkey]. MTA Report, No. 123–124, pp. 67–89.

Claypool, G.E., Holzer, W.T., Kaplan, I.R., Sakai, H., Zak, I., 1980. The age curves of sulfur and oxygen isotopes in marine sulfate and their mutual interpretation. Chem. Geol. 28, 199–260.

Deb, M., Hoefs, J., Boumann, A., 1991. Isotopic composition of two Precambrian stratiform barite deposits from the Indian shield. Geochim. Cosmochim. Acta 55, 303–308.

Dolgov, Yu.A., Bazarov, L.Sh., Bakumenko, I.T., 1968. Metod of determination of pressure in inclusions by means of simuitaneus use of homogenization and cryometry, in: Mineralogical Thermometry and Barometry [in Russian]. Nedra, Moscow, Vol. 2, pp. 9–17.

Evensen, N.M., Hamilton, P.J., O'Nions, R.K., 1978. Rare earth abundances in condritic meteorite. Geochim. Cosmochim. Acta 42, 1199–1212.

Faure, G., 1977. Principles of Isotope Geology. John Wiley and Sons Inc., New York, pp. 107–137.

Faure, G., 1986. Principles of Isotope Geology, second ed. John Wiley and Sons Inc., New York.

Fazakas, H.J., 1976. Geochemisch-Lagesttaettenkundliche Untersuchungen an Schwerspatvorkommen des Sьdwestdeutschen Grund und Deckgebirges. Naturwiss. Fak., Univ. Mьnchen, Doktora Tezi.

Fu, B., Aharon, P., 1997. Origin and depositional model of barite deposits associated with hydrocarbon seeps on the Gulf of Mexico slope. Gulf Coast Association of Geological Societies Transactions 46, 125–131.

Galindo, C., Tornos, F., Darbshire, D.P.F., Casquet, C., 1994. The age and origin of the barite-fluorite (Pb–Zn) veins of the Sierra Del Guadarrama (Spanins central system Spain): a radiogenic (Nd, Sr) and stable isotope study, Isotope geoscience section. Chem. Geol. 112, 351–364.

Hanor, J.S., 2000. Barite–celestine geochemistry and environments of formation, in: Alpers, C.N., Jambor, J.L., Nordstrom, D.K. (Eds.), Reviews in Mineralogy and Geochemistry, Vol. 40: Sulfate Minerals: Crystallography, Geochemistry and Environmental Significance. Min. Soc. Am., Washington, D.C., pp. 193–275.

Holland, H.D., 1984. The Chemical Evolution of the Atmosphere and Oceans. Princeton Univ. Press, Princeton, NJ.

Kayabali, I., 1992. Geological, genetic and petrologic investigation of the barite Alanozu, Habiller (Karaman) area. Suleyman Demirel University, Ph.D. Dissertation.

Kesler, S.E., Jones, L.M., 1981. Sulfur and strontium isotopic geochemistry of celestite, barite and gypsum from the Mesozoic basins of North-Eastern Mexico. Chem. Geol. 31, 211–224.

Klevtsov, P.V, Lemmlein, G.G., 1959. Presure corrections for the homogenization temperatures of agueous NaCl solutions. Dokl. Akad. Nauk SSSR 128, 1250–1253 [Translated in Am. Geol. Inst., Acad. Sci. SSSR Dokl. 128 (1960), 995–997].

Kupeli, S., Ayhan, A, Karadag, M.M., Arik, F., Doyen, A., Zedef, V., 2006. C, O, S and Sr isotope studies of siderite mineralization in the Atepe (Feke-Adana) iron deposits and genetic findings. TJK Abstract, Ankara, 143–144.

Marumo, K., 1989. The barite ore fields of kuroko type of Japan, in: De Brodtkorb, M.K. (Ed.), Non-Metalliferous Stratabound Ore Fields. Van Nostrand Reinhold, New York, pp. 201–231.

Michard, A., Albarede, F., 1986. The rare content of some hydrothermal fluids. Chem. Geol. 55, 51–60.

Ohmoto, H., 1986. Stable isotope geochemistry of ore deposits, in: Valley et al. (Eds.), Stable Isotopes in High Temperature Geological Processes. Reviews in Mineralogy, Vol. 16, pp. 491–559.

Ohmoto, H., Rye, R.O., 1979. Isotopes of sulfur and carbon, in: Barnes, H.L. (Ed.), Geochemistry of Hydrothermal Ore Deposits, second ed. Wiley, New York, pp. 509–567.

Ozgul, N., Kozlu, H., 2002. Stratigraphy and findings related to structural location of Kozan-Feke (Dogu Toroslar) area. TPJD Bull. 14 (1), 1–36.

Ozus, A.S., Yaman, S., 1986. Fluorite–barite mineralization and origin issues of Akaya (Feke–Adana). Bull. Geol. Soc. Turk. 29, 35–42.

Paytan, A., Mearon, S., Cobb, K., Kastner, M., 2002. Origin of marine barite deposits: Sr and S isotope characterization. Geology 30, 747–750.

Podufal, P., 1977. Die Dreislarer Barytange. Der Aufschluss 55, Beiheft 2, 37–40.

Puchelt, H., 1967. Zur Geochemie des Bariums im exogenen Zyklus. Sitzungsber., Heid., Ak. Wiss., Math. Nat. Kl., Jg., 4 Abh., p. 205.

Reimer, T., 1978. Detrital barites in Karoo Supergroup of Southern Africa. Miner. Deposita 13, 235–244.

Ronov, A.B., Balashov, Y.A., Migdisov A.A., 1967. Geochemistry of the rare earths in the sedimentary cycle. Geochem. Int. 4, 1–17.

Rye, R.O., Ohmoto, H., 1974. Sulfur and carbon isotopes and ore genesis: A review. Econ. Geol. 69, 826–842.

Starke, R., 1969. Die Strontiumgehalte der Baryte. Freiberger Forschungsh. 150, p. 86.

Sharma, R., Verma, P., Sachan, H.K., 2003. Strontium isotopic constraints for the origin of barite mineralization of Tons Valley, Lesser Himalaya. Research Communications. Current Science 85 (10), 653–656.

Striebel, H., 1965. Die Bleierz-Baryt-Lagerstaette von Karalar-Gazipasa (Turkei) und ihr geoiogischer Rahmen. Naturwiss. Fak. Univ. Mьnchen, Ph.D. Dissertation.

Uras, Y., Oner, F., Yaman, S., 2003. Geochemie des Fluoritvorkommens von Feke (Adana-Tьrkei) im Osten des Taurusgebirges. Chemie der Erde— Geochemistry 63, 55–62.

Werner, C.D., 1958. Geochemie und paragenese der saxonischen schwerspat–flussspat–gдnge im schmalkaldener revier. Freiberger Forschungshf 47, Berlin.

Zimmermann, R.A., 1976. Rhythmicity of barite-shale and of Sr in stratabound deposits of Arkansas, in: Wolf, K.H. (Ed.), Handbook of Stratabound and Stratiform Ore Deposits. Elsevier, Vol. 3 pp. 339–353.

Рекомендована к печати 30 марта 2017 г.
А.Э. Изохом

Поступила в редакцию 25 февраля 2016 г.,
после доработки — 13 февраля 2017 г.